Research paper

Struct Multidisc Optim 26, 326–332 (2004)
DOI 10.1007/s00158-003-0313-8

Interface study and boundary smoothing on designed composite material microstructures for manufacturing purposes

H. Qi, N. Kikuchi and J. Mazumder

Abstract The manufacturability of composite material microstructures designed by the homogenized topology optimization method has to be considered when bringing the design into reality. In this paper, numerical studies are conducted on multiphase material microstructures that have negative coefficients of thermal expansion, for the purpose of improving manufacturability. Realistic manufacturing factors are considered, including the diffusion interface between two constituent phases and vectorized toolpath design. The effect of the mixture interface between two solid phases is examined by homogenization analysis. An image-processing program is developed to smooth out the boundaries of the topological structure to facilitate toolpath design. Numerical results show that the diffusion interface between two solid material phases reduces the effective negative thermal expansion property of the whole microstructure. The designed material properties are retained and converge after boundary smoothing.

Key words topology optimization, composite material, bimetallic interface, boundary smoothing

1 Introduction

Composite material microstructures created by the homogenized topology optimization design (HTOD) method (Fujii *et al.* 2001) are able to achieve unusual material properties, such as negative Poisson's ratios (Sigmund 1995) and negative coefficients of thermal expansion (Sigmund and Torquato 1997). This type of material design, a departure from the conventional material selection methods with which performance is limited by the available materials, has drawn much attention in mechanical, environmental, and biomedical engineering applications. However, very little literature is available discussing the manufacturability of such designed material microstructures.

Solid freeform fabrication (SFF) techniques are able to make the design and fabrication of metallic parts faster and more cost efficient. Nowadays, the laser-facilitated SFF process, i.e. the direct metal deposition (DMD) technique (Mazumder *et al.* 1999), is not only able to fabricate with fine resolution from pixel to pixel, but is also capable of fabricating multiple materials simultaneously. This advance opens the area of creating the new class of optimally designed material microstructures.

However, the manufacturability of optimally designed material microstructures has to be improved when bringing the design into reality. In homogenized topology optimization design, the output topological microstructure is represented by an element-based image. In order to save computing time, designed material microstructures are usually optimized by discretizing the design domain with coarse finite elements. Therefore, the structure, which is composed of square elements, may lose some detailed geometrical information due to the zigzag mosaic effect. From a manufacturing perspective, this discretized topology information needs to be converted into vectorized toolpath information that can be ultimately downloaded to a CNC system. In order to enhance the fabrication resolution, the boundaries of the microstructure have to be smoothed by a curve-fitting technique. In this way, the element-based image can be converted into a vectorized image in which the regions of different material phases are enclosed by vectorized curves. Such a file can be imported into CAD software for toolpath generation. Then the toolpath design is adjusted based on the optimized SFF processing parameters from statistic-based experiments.

Previous research work conducted in the Department of Mechanical Engineering at the University of Michigan has combined the two state-of-the-art technologies successfully, namely the DMD technique and the HTOD

Received: 14 May 2003
Published online: 7 October 2003

H. Qi, N. Kikuchi ✉ and J. Mazumder

Department of Mechanical Engineering, University of Michigan, Ann Arbor, Michigan 48109–2125, USA
e-mail: qih@umich.edu, kikuchi@umich.edu, mazumder@umich.edu

material design methodology. An optimally designed material microstructure that has a negative coefficient of thermal expansion (NCTE) material property was manufactured by the direct metal deposition technique (Mazumder *et al.* 2000). Nickel and chromium were selected as the two constituent materials for the NCTE microstructure. The NCTE sample exhibited a contraction behavior when tested under a rising temperature up to 100 °C.

The DMD process, like other prototyping processes that use a concentrated heat source to melt deposited materials, may inevitably introduce a mixture phase between two deposited materials. This mixture phase is obviously not desired for the design. However, manufacturing problems such as bimetallic interface porosities and cracks occurred in the aforementioned NCTE sample as a result of trying to avoid such mixture interfaces. Imperfect metallurgical bonding could result in deviations from the expected material properties. Since metallic materials are not likely to bond without metallurgical diffusion using most manufacturing methods, the HTOD method has to be able to take into account the interface effect in the optimal design stage.

In this paper, examples of multiphase material microstructures designed by the homogenized topology optimization method are studied for improvements in manufacturability. Homogenization analysis is performed on the interface-incorporating NCTE structures to investigate the interface effect. An image-processing program is developed to smooth out the boundaries of the topological microstructure.

2
Designed material microstructure

Two-dimensional NCTE microstructures designed by the HTOD method were adopted in this study. In both examples, the thermal elasticity properties were engineered by three material phases, i.e. two solid phases and one void phase. The first solid phase material had a Young's modulus of $E_1 = 1.0$, a Poisson's ratio of $\nu_1 = 0.3$, and a coefficient of thermal expansion of $\alpha_1 = 1.0$, whereas the second solid phase had the same Young's modulus of $E_2 = 1.0$ and Poisson's ratio of $\nu_2 = 0.3$, but a different coefficient of thermal expansion of $\alpha_2 = 10.0$. The third phase was a void material with a very small Young's modulus of 10^{-4} in order to avoid the singular matrix condition when solving the system equations. The artificial material mixture method (Bendsøe 1989) was used to distribute the three constituent material phases, i.e.,

$$\mathbf{C}^{(e)}\left(m^{(e)}, d^{(e)}\right) = \left(d^{(e)}\right)^{p}\left[m^{(e)}\mathbf{C}_1 + \left(1 - m^{(e)}\right)\mathbf{C}_2\right], \tag{1}$$

where $\mathbf{C}^{(e)}$ is an elementary material property, e.g. the elasticity or thermal stress, $m^{(e)}$ and $d^{(e)}$ are elementary design variables representing the mixture fraction of the two solid phases and the density fraction of the solid and void phases, respectively, and p is a penalization factor.

The optimal material microstructure was designed to have the effective material property of a negative coefficient of thermal expansion. The unit cell was considered as isotropic with a square-symmetry density distribution. Under the plane stress assumption, the target material properties of the first example were $\alpha_{11} = -6.0$ and $\alpha_{22} = -6.0$, subject to volume constraints of $V_1 = 30\%$ and $V_2 = 30\%$. The optimization problem formulation can be stated as

$$\min_x \left[\alpha_{11}^H - (-6.0)\right]^2 + \left[\alpha_{22}^H - (-6.0)\right]^2, \tag{2}$$

s.t. there is a 30% volume constraint for each solid phase, and square symmetry.

The optimized microstructure in a base cell and the composite materials composed of a 3×3 array of the base cells are shown in Fig. 1, in which the area of dark color represents solid phase one and the area of light color represents solid phase two. The effective properties were

$$\mathbf{E}^H = 0.01\begin{bmatrix} 3.51 & -0.59 & 0 \\ -0.59 & 4.85 & 0 \\ 0 & 0 & 0.96 \end{bmatrix},$$

$$\boldsymbol{\alpha}^H = \begin{bmatrix} -6.276 & 0 \\ 0 & -6.529 \end{bmatrix}.$$

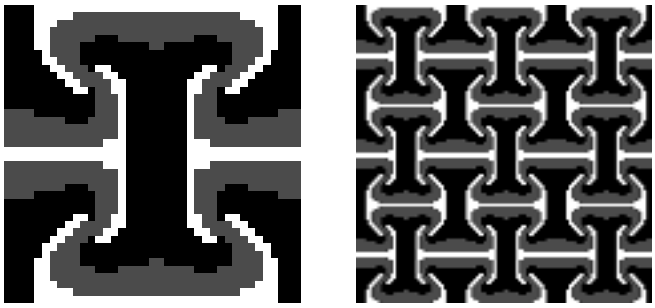

(a) Unit cell mesh 40×40 (b) Array 3×3

Fig. 1 NCTE microstructure Example 1

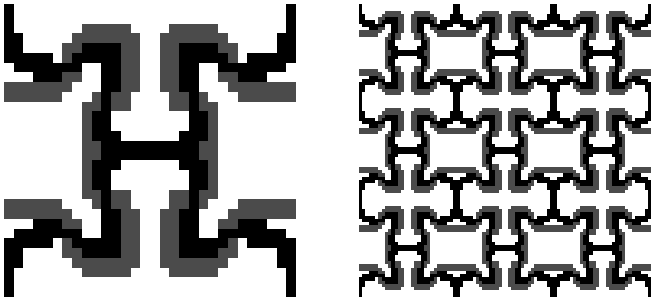

(a) Unit cell mesh 30×30 (b) Array 3×3

Fig. 2 NCTE microstructure Example 2

The second example (Chen *et al.* 2001) had the same target material properties and square-symmetric geometry but was subject to volume constraints of $V_1 = 20\%$ and $V_2 = 20\%$ and a positive Poisson's ratio (shown in Fig. 2). The effective properties were

$$\mathbf{E}^H = 0.01 \begin{bmatrix} 1.29 & 0.43 & 0 \\ 0.43 & 1.72 & 0 \\ 0 & 0 & 0.39 \end{bmatrix},$$

$$\boldsymbol{\alpha}^H = \begin{bmatrix} -7.354 & 0 \\ 0 & -6.047 \end{bmatrix}.$$

3 Interface study

Homogenization analysis was conducted on the two NCTE structures to examine the effect of a mixture interface on the effective structural properties. The mixture phase was constructed with 50% of solid phase one and 50% of solid phase two. The interface width was set to be the size of two elements across the interface. Therefore, the interface width decreases when the mesh size is refined, as shown in Fig. 3. The results (Table 1) show that the introduced mixture interface between the two solid phases generally increases the designed material property – the negative coefficient of thermal expansion changes in the positive direction. It can also be observed that the homogenized thermal elastic properties of the microstructure are mesh independent.

Another parametric study was conducted by considering the microstructures of NCTE 1 in a 116×116 mesh and NCTE 2 in a 120×120 mesh, while the interface width was varied by setting the number of element across the interface. The results are plotted in Fig. 4. The coefficients of thermal expansion of the NCTE microstructures increase almost linearly with increasing interface width.

In order to explain the interface effects on NCTE structures, a two-dimensional cantilever beam model, as shown in Fig. 5a, was built in ABAQUS/CAE. Its size

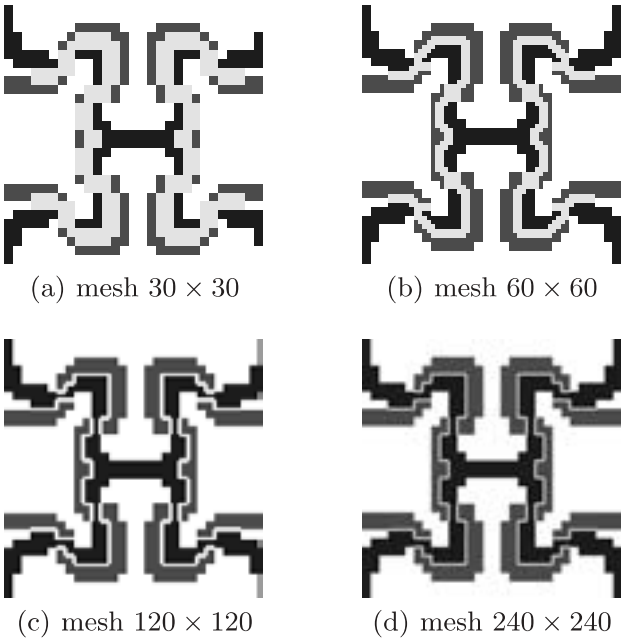

Fig. 3 Interface width changes with element size

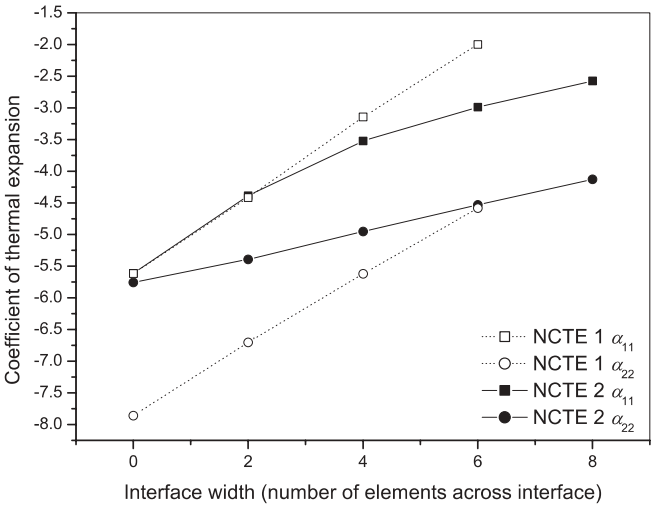

Fig. 4 Interface width effect on NCTE 1 (116×116 mesh) and NCTE 2 (120×120 mesh) microstructures

Table 1 Interface effect on NCTE microstructure 2

Mesh	Interface	E_{1111}	E_{2222}	E_{1212}	α_{11}	α_{22}
30×30	No	0.0129	0.0172	0.0039	−7.354	−6.047
	Yes	0.0129	0.0172	0.0039	−2.123	−5.354
60×60	No	0.0127	0.0167	0.0038	−6.662	−5.969
	Yes	0.0127	0.0167	0.0038	−3.448	−5.706
120×120	No	0.0125	0.0165	0.0037	−6.510	−5.965
	Yes	0.0125	0.0165	0.0037	−4.631	−5.952
240×240	No	0.0125	0.0164	0.0037	−6.481	−5.976
	Yes	0.0125	0.0164	0.0037	−5.429	−6.020

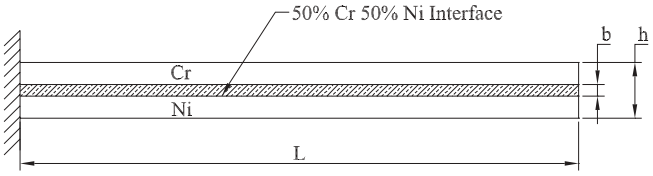

(a) Ni-Cr beam set-up.

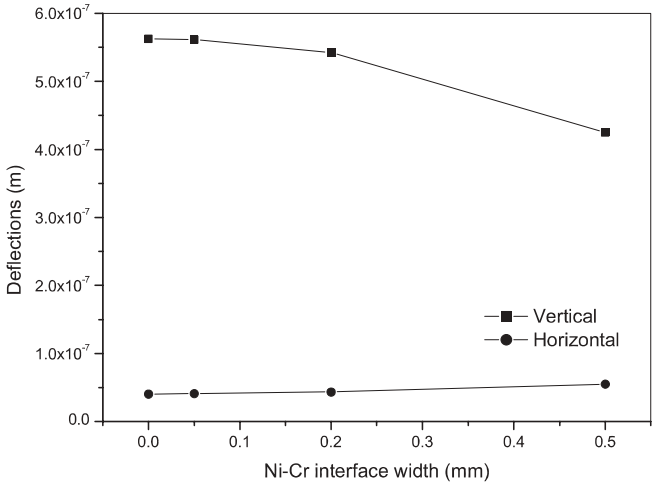

(b) Free end deflection due to unit temperature rise.

Fig. 5 Interface effect on the stiffness of the Ni–Cr cantilever beam under thermal load

was approximated as the smallest feasible size that could be manufactured by the DMD process. The length of the beam L was 10 mm and the width h was 1 mm. The beam was composed of chromium and nickel. A mixture of 50% of each material was assumed at the interface. The width of the interface b changed from zero to 0.5 mm as an input variable. Because nickel has a greater coefficient of thermal expansion than chromium, the beam bends when subjected to a uniform temperature rise. The free end deflection due to a unit temperature change was examined for different interface widths. As shown in Fig. 5b, the deflection in the vertical direction, which is the major magnitude of the free-end deflection, was found to decrease when the width of the mixture-phase interface increased. In other words, the composite beam becomes stiffer when the mixture interface is thickened. The NCTE structure has the ability to shrink when heated due to the bimetallic-strip behavior of the nickel and chromium. The mixture interface reduces the bending effect. Therefore, it will reduce the contraction deformation of the NCTE structure when heated.

4 Boundary smoothing

An accurate nonlinear curve-fitting scheme was developed to smooth the continuous boundaries of the NCTE microstructures. The effective material properties, after the boundary smoothing, were expected to have relatively small discrepancies from the original design and to show a convergent trend. The boundary points were curve-fitted by Bezier functions up to 15th order depending on the number of sampling points. For the three-phase NCTE microstructure, the boundaries between the solid phases and the void phase (S/V) were curve-fitted within the entire base cell domain first, then the boundaries between the two solid phases (S/S) were curve-fitted within the solid phase domain. In order to check the effective material properties after boundary smoothing, boundary points were reconstructed on the refined mesh, and phase information was reassigned to the points inside the boundaries. The density distribution file was output to evaluate the new material properties. The entire boundary-smoothing program could be divided into six subprograms according to the function each of them achieved. These subprograms and their functions are described below:

Step 1 Identify elements on boundaries.
In the first step, the density distribution of the designed microstructure is read from the optimization results. The symmetry of the structure is detected. For simplicity, only a part of the symmetrical structure in the base cell is considered in the subsequent processes. According to (1) the elementary density and mixture fractions are filtered to integers that represent the three constituent phases. Elements on the solid phase boundaries are detected first. Then the elements on the interfaces between the two solid phases are detected (Fig. 6).

Step 2 Sort boundary elements.
In this step, the detected boundary elements are sorted into groups and rearranged in the connecting sequence along the boundary. In this

Fig. 6 Boundary elements are detected on the quarter part of the square symmetric structure

way, phase boundaries can be outlined by jointed points.

Step 3 Curve-fit with Bezier function.

The vectorized boundary curve can be approximated by the polynomial expression

$$\mathbf{r} = \sum_{i=1}^{n} \boldsymbol{\alpha}_i B_i(\theta)\,, \tag{3}$$

where $\boldsymbol{\alpha}_i$ is a set of coefficients corresponding to the ith order of the basis function $B_i(\theta)$. The least- squares method is implemented in solving for $\boldsymbol{\alpha}_i$. The basis polynomial function used here is the Bezier function defined as

$$B_i(\theta) = \frac{n!}{(i-1)!(n-i+1)!}\theta^{i-1}(1-\theta)^{n-i+1}\,, \tag{4}$$

where n is the order of the Bezier function, i is an index from 1 to $n+1$, and θ is a dimensionless variable defined on the interval $[0, 1]$. The order of the Bezier function is determined by the number of sampling points (Table 2).

The S/V boundaries are curve-fitted first. The junction points of the S/V and S/S boundaries have to be relocated on the newly generated S/V curves. Then, these junction points are added into the sampling points for S/S boundary curve-fittting. The results are shown in Fig. 7.

Step 4 Reconstruct boundary points on refined mesh.

The mesh is refined by inserting nodal points between the original neighboring nodal points, i.e. a $m \times m$ mesh will be refined to a $[p(m-1)+1]\times[p(m-1)+1]$ mesh, where p is the number of times the mesh has been refined. The new boundary points falling on the refined mesh are selected as the nearest point to the Bezier curves. Every sequential point along the boundary is determined by finding the minimum point-to-curve distance among the eight neighbor points surrounding the previous point. An eight-direction chain code is created for each boundary curve. Figure 8 shows the reconstructed boundary points on a refined mesh.

Table 2 Relationship between the order of the Bezier function and the number of curve-fitting points

Number of points	Order of Bezier function
< 3	(N/A)
3–10	4
11–20	8
21–40	12
> 40	15

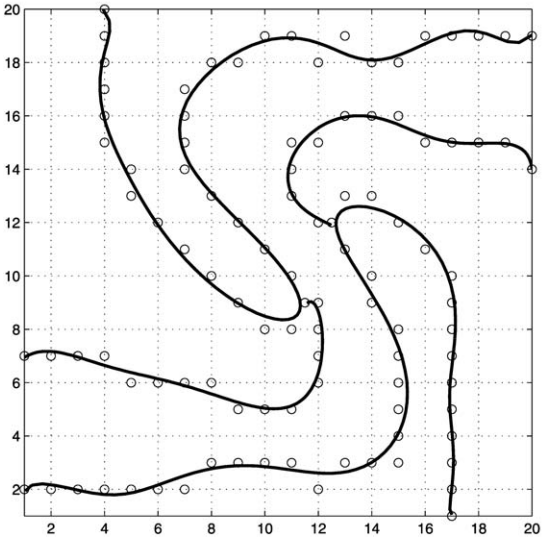

Fig. 7 Curve-fitting on boundary points using the Bezier function

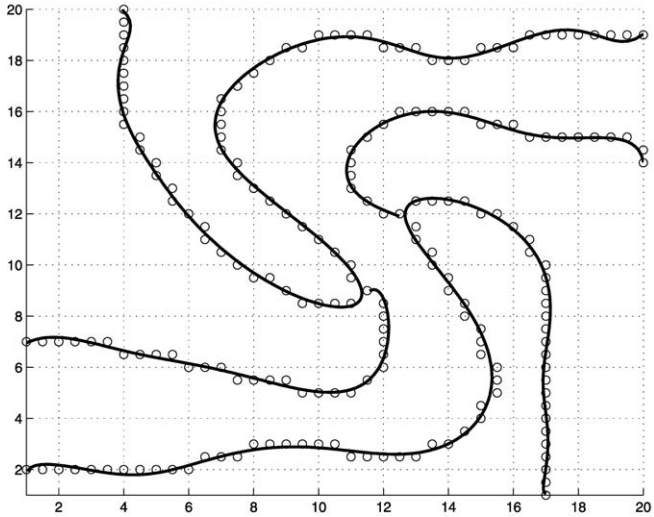

Fig. 8 Reconstructed boundary points on a refined mesh

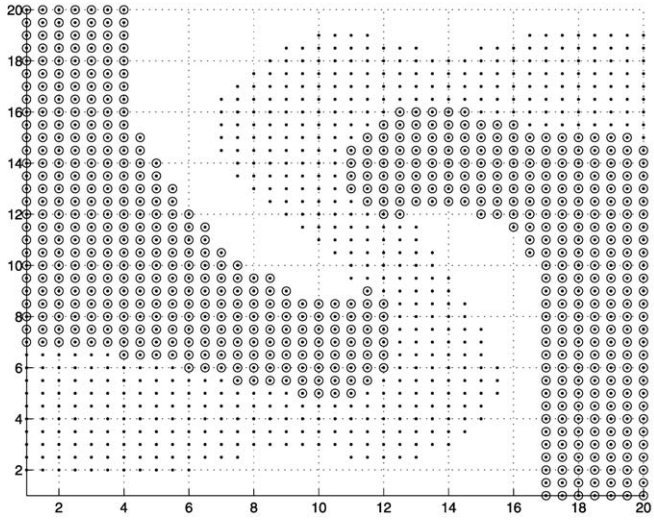

Fig. 9 Fill phases in different regions

Step 5 Fill in phases.
The solid phase is filled first within the S/V boundaries by assigning the elements with indicative integers. Then, within the S/S and S/V boundaries, solid phase one is filled. The rest of the elements are characterized by solid phase two. An image-processing filling scheme called the seed-fill-scan-line algorithm is used to 'paint' the different phases (Fig. 9).

Step 6 Output density distribution.
In the last step, the symmetry of the structure is recovered. The indicative phase integers are converted to density and mixture fractions for each element and output as a density distribution file ready for homogenization analysis. The results of boundary-smoothed NCTE microstructures in different refined meshes are shown in Figs. 10 and 11.

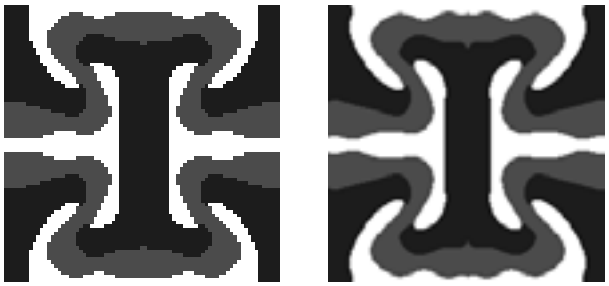

(a) mesh 78 × 78 (b) mesh 192 × 192

Fig. 10 Boundary-smoothed NCTE microstructure 1

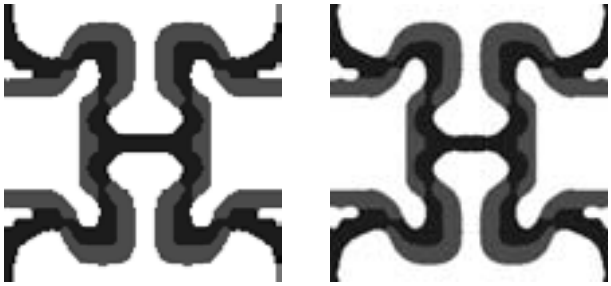

(a) mesh 120 × 120 (b) mesh 238 × 238

Fig. 11 Boundary-smoothed NCTE microstructure 2

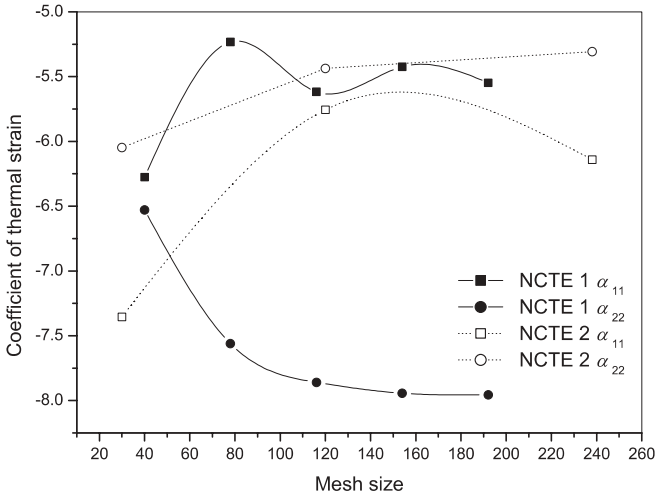

Fig. 12 Effective thermal strains of NCTE microstructures vs. mesh size

The two boundary-smoothed NCTE microstructures were examined by homogenization analysis on the effective material properties. Figure 12 shows the original designed material property – the negative coefficient of thermal expansion is retained well when the mesh size is refined. It also shows a converging trend as the boundary is smoothed on the refined mesh.

5 Conclusions and discussion

From this numerical study, the following conclusions can be drawn:

(1) The mixture interface between two solid material phases reduces the effective negative thermal expansion property of the whole microstructure in the positive direction.
(2) The effective material properties are retained well and converge when the mesh is refined after boundary smoothing.

These preliminary numerical results need to be verified by a real SFF process. Two research directions can be identified hereafter. One is to improve the SFF manufacturing technique to manufacture the multiphase material microstructure. Another is to take the factors of the manufacturing process into account at the HTOD design stage. Interface-incorporating material microstructure design will be developed. A secondary topology optimization inside the interface region can be performed in order to minimize the mismatch between the original design and the interface-incorporating design.

Combined with SFF experimental data, interface modeling can be improved in the HTOD method. The mixture interface was assumed to be a uniform mixture phase with 50% of each constituent phase. This assumption is not realistic for a laser-induced SFF process, due to the complicated bimetallic solidification process involved in a real situation. Bimetallic interface properties will be further studied from SFF experiments. A porosity-free and uniform mixture interface is sought. The modeling of solidification physics such like bimetallic binary phase miscibility may be considered. Since the solidification of a bimetallic interface can be controlled by the SFF process as a processing parameter, the effective material property can be controlled by the manufacturing process directly.

This design and manufacturing integrated scheme will be implemented for the more practical design of

three-dimensional composite material microstructures with combined material properties, such as low-thermal-expansion and high-conductivity materials.

Acknowledgements The authors would like to acknowledge financial support from DARPA/NIST (Grant No. F000763) for this work.

References

Bendsøe, M.P. 1989: Optimal shape design as a matrial distribution problem. *Struct. Multidisc. Optim.* **1**, 193–202

Chen, B.C.; Silva, E.; Kikuchi, N. 2001: Advances in computational design and optimization with application to MEMS. *Int. J. Numer. Methods Eng.* **52**, 23–62

Fujii, D.; Chen, B.C.; Kikuchi, N. 2001: Composite material design of two-dimensional structures using the homogenization design method. *Int. J. Numer. Methods Eng.* **50**(9), 2031–2051

Mazumder, J.; Schifferer, A.; Choi, J. 1999: Direct materials deposition: designed macro and microstructure. *Mater. Res. Innov.* **3**(3), 118–131

Mazumder, J.; Dutta, D.; Kikuchi, N.; Ghosh, A. 2000: Closed loop direct metal deposition: art to part. *Opt. Lasers Eng.* **34**(4–6), 397–414

Sigmund, O. 1995: Tailoring materials with prescribed elastic properties. *Mech. Mater.* **20**(4), 351–368

Sigmund, O.; Torquato, S. 1997: Design of materials with extreme thermal expansion using a three-phase topology optimization method. *J. Mech. Phys. Solids* **45**(6), 1037–1067